

## ARTICLE

# Characterization and radioactive evaluation of the concrete from a radiotherapy bunker

Marta Torres-González<sup>1,2</sup> | Juan Mantero<sup>3</sup> | Santiago Hurtado<sup>3</sup> |  
Vicente Flores-Alés<sup>1</sup>  | Francisco J. Alejandro<sup>1</sup> | Juan M. Alducín-Ochoa<sup>1</sup>

<sup>1</sup>Department of Architectural  
Constructions II, Universidad de Sevilla,  
Seville, Spain

<sup>2</sup>Department of Civil Engineering,  
Architecture, and Georesources, IST,  
University of Lisbon, Lisboa, Portugal

<sup>3</sup>Applied Physic II Department,  
Universidad de Sevilla, Seville, Spain

## Correspondence

Vicente Flores-Alés, Avda. Reina  
Mercedes n°4, 41012 Seville, Spain.  
Email: vflores@us.es

## Funding information

Ministerio de Ciencia, Innovación y  
Universidades, Grant/Award Number:  
PGC2018-093470-B-I00

## Abstract

The construction of concrete structures for radiological protection in sanitary facilities requires a series of constructive conditions that guarantee safety. The influence of the correct bunkers design, wall thicknesses and the type of materials used is essential to ensure effective protection. The use of barite aggregate concrete is a common resource to improve the radiation attenuation capacity of concrete walls. The present study analyses the structure of a bunker during a renovation work, studying the construction characteristics of the chamber, the state of its elements, the characterization of materials, the identification of the emissions of the possible isotopes present, beta radioactive contamination and the measurement of equivalent dose rates at different points in the concrete. The results made it possible to determine the use of conventional concrete and barite concrete, the latter presenting a BaO content of around 40% and particularly low resistance values, not observing alteration processes in the materials.

## KEYWORDS

barite concrete, gamma spectrometry, ground penetration radar, radioactivity

## 1 | INTRODUCTION

Radiotherapy equipment is equipped with radiation sources that base their action on photon and electron beams produced in linear accelerators.<sup>1</sup> They operate with high energy at voltages above 6 MV, generating neutrons in significantly high doses for exposed persons<sup>2</sup> and

also high levels of absorbed dose.<sup>3</sup> That is the reason why they are located in concrete chambers, sometimes underground, which can be more than 1 m thick. The concrete performs as insulation, preventing possible radioactivity emissions to the outside, beyond the shielding of the equipment itself.

Depending on the radiation intensity that will be generated inside these chambers, commonly known as bunkers, the radioactive protection characteristics are determined by the thickness and density of the concrete wall. Additionally, in some cases, high-density heavy concrete is used to reinforce the insulating and

Discussion on this paper must be submitted within two months of the print publication. The discussion will then be published in print, along with the authors' closure, if any, approximately nine months after the print publication.

This is an open access article under the terms of the Creative Commons Attribution-NonCommercial-NoDerivs License, which permits use and distribution in any medium, provided the original work is properly cited, the use is non-commercial and no modifications or adaptations are made.

© 2022 The Authors. Structural Concrete published by John Wiley & Sons Ltd on behalf of International Federation for Structural Concrete

attenuation capacity of the chamber. These concretes must have a density of over  $3000 \text{ kg/m}^3$  to guarantee their effectiveness.<sup>4</sup> The most commonly used resource to reach these density values is the replacement of conventional aggregate by barite (average density  $4.48 \text{ g/cm}^3$ ),<sup>5</sup> allowing a significant increase in the density of the concrete.<sup>6,7</sup> According to Topçu, the most favorable water/cement ratio (w/c) for heavyweight concrete used for the prevention of leakage from radioactive structures due to the harmful effect of radioactive rays to living bodies is 0.40 and the cement dosage should not be lower than  $350 \text{ kg/m}^3$ . Anyway, the compressive strength is not a predominant factor because of the thickness of the radiation shields and the use of high-quality concrete in the mixtures.<sup>8</sup> It is important to note that, due to the weight of the aggregates, in heavy concretes there is a risk of segregation during placing, which requires short mixing times and an increase in the proportion of fine aggregates.<sup>8</sup>

The safety factors considered in the design of these constructions should take into account an overestimation of the workload, the voltages of the equipment to be accommodated, the occupancy and user levels and the size of the radiation field. In addition, the direct incidence of the beam, the presence of people next to the wall on the other side of the shielding and the most unfavorable points of the shielding, such as installation connection points, junctions, doors, observation openings, etc., should be also considered. The thickness of the walls should be calculated based on the linear attenuation coefficients<sup>9</sup> whose increase is directly proportional to the barite concentration in concrete.<sup>10</sup> Furthermore, it is important to evaluate the size and quantity of barite aggregates to optimize the attenuation.<sup>11</sup>

In the case of linear accelerators (LINAC), electrons can reach energies between 6 and 25 MeV, which are then transformed into X-rays for therapeutic purposes. These X-rays eventually reach energies of more than 10 MeV, which can induce both photonuclear ( $\gamma, n$ ) and electronuclear ( $e, e'n$ ) reactions.<sup>12</sup> Consequently, as a result of these reactions, fast neutrons and the activation of different radioisotopes are produced in the materials located in the treatment room. The main sources of neutrons come from the accelerator head components (collimators, filters, ...), originating from stainless steel elements, such as Mn, Ni, Co, and Al, and producing radioisotopes with short half-lives,<sup>13</sup> some of these neutrons reach the concrete walls of the accelerator bunker undergoing elastic collisions with the nuclei of the constituent materials. Thus, the impurities present in the concrete, which are highly dependent on the aggregates used for their manufacture, will be critical for the activation of different radioisotopes. Traces of stable europium

(Eu), cobalt (Co), and cesium, (Cs) which are normally present in concrete, are converted into long-lived activated products such as the gamma emitters Eu-152, Co-60, and Cs-137<sup>14</sup> with a half-life of 13.5, 5.3, and 30.23 years, respectively. The most relevant aspect of the presence of these impurities is that a possible declassification of the concrete would be delayed to about 10 years if Eu-152 is detected and, to a lesser extent, in the case of Co-60 an average lifespan of 5.3 years. Conversely, activation of the radioisotope Cs-137 would further increase the cooling period.<sup>15</sup> Activation of the beta emitter C-14 on the surface of concrete walls with a half-life of 5730 years is also possible.<sup>16</sup> In the specific case of barite concrete used as shielding, which contains barite bound in a Portland cement matrix, the radioisotope that can be activated is Ba-133.<sup>17</sup>

## 2 | INFRASTRUCTURE STUDIED

The infrastructure studied consists of a bunker located in a hospital in Seville (Spain). It was built with reinforced concrete to house a linear accelerator for cancer treatment used annually by more than 2000 patients. This bunker is located on the ground floor, being in direct contact with the ground, with no room on the upper floor. One of its walls is part of the building's façade and the three remaining walls are adjacent to other rooms or the lobby.

The interior layout of the bunker, the dimensions and the constructive configuration have been designed in accordance with the requirements necessary to enable the correct mechanical installation of the accelerator and to ensure its functionality for patients and operators, taking into account the criteria contained in the radiation protection study approved by the Nuclear Safety Council (<https://www.csn.es/documents/10182/914805/La+protecci%C3%B3n+radiol%C3%B3gica+en+el+medio+sanitario>).

The room has a free height of 3 m and a surface area of  $43.9 \text{ m}^2$ . It is divided into two spaces, of which  $18.6 \text{ m}^2$  correspond to the access labyrinth, which is required by standards for the construction of this type of room,<sup>18</sup> and  $25.5 \text{ m}^2$  to the chamber itself, which houses the linear accelerator (Figure 1). The wall thicknesses vary between 111 and 157 cm. The paving slab does not have a relevant edge as it is in direct contact with the ground (Figures 1 and 2).

The possibility of studying the reinforced concrete used in the construction of this bunker arises from the fact that a DBX (small diagnostic biopsies) linear accelerator for radiotherapy treatments, whose nominal energy is 6 MV and its maximum radiation field is  $40 \times 30 \text{ cm}$ ,

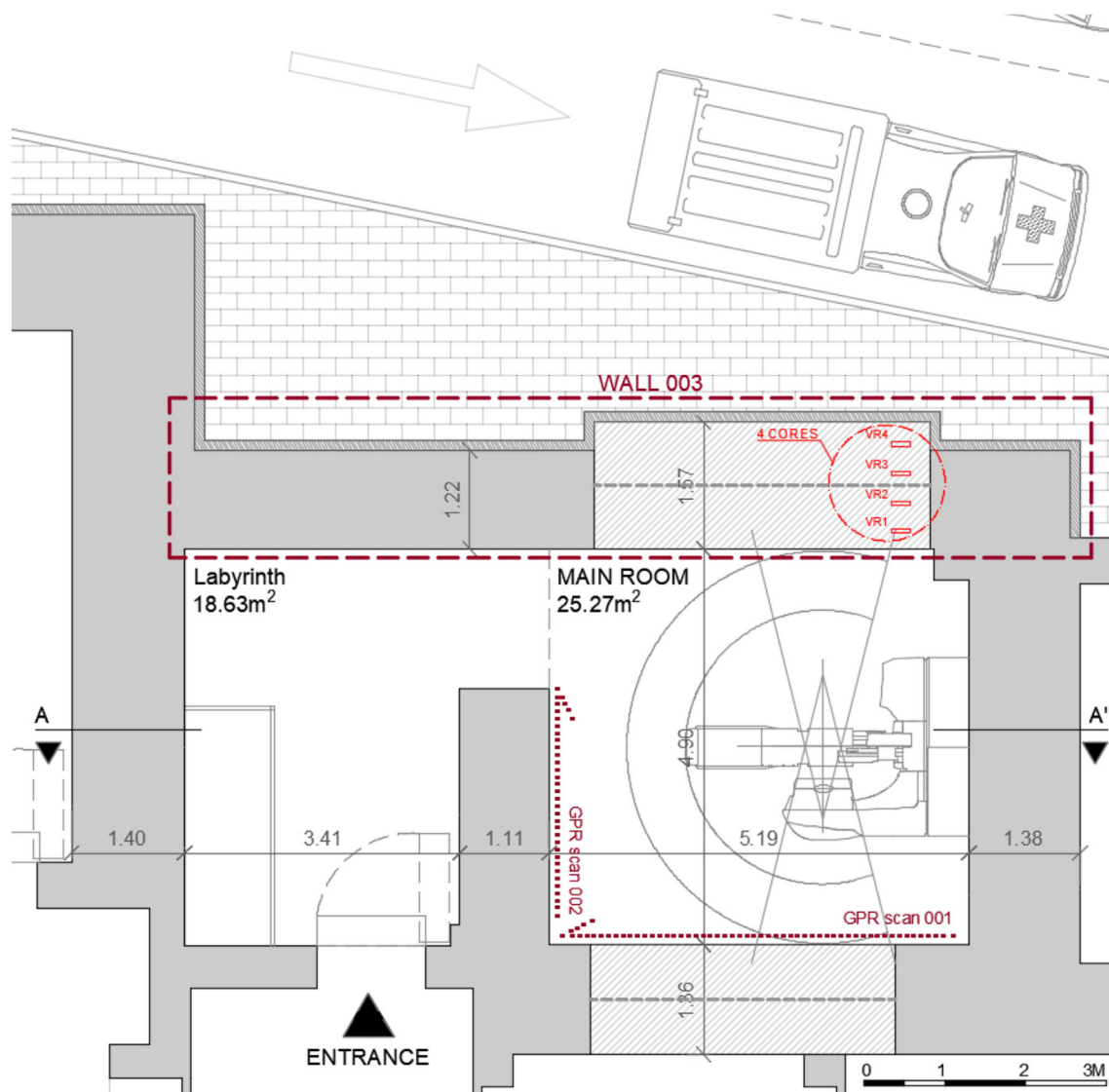


FIGURE 1 Bunker floor plan

has been replaced by a new equipment with higher performance (Figure 3a).

Due to the dimensions of the new equipment, it was necessary to adapt the bunker to comply with the criteria established in the regulations.<sup>19</sup> To do this, it was necessary to completely dismantle wall 003 by cutting with steel wire (Figure 3b). One of the doubts, prior to the study, was centered on the characteristics of the concrete used. There was not enough information on the subject, although some documents stated the use of barite concrete. This intervention made it possible to observe that part of the wall of the chamber was composed of two sheets of different concretes. This arrangement of the wall with two bonded sheets confirms the hypothesis, which has not been documented, that the chamber has a reinforcement ring in the area of direct incidence of

radiation. This ring is composed by an inner sheet of conventional concrete and an outer sheet of barite concrete that runs along wall 001, the roof and wall 003 (Figures 1 and 2), not being necessary in the pavement as the radiation is dissipated in the ground.

With regard to the steel reinforcement, the work carried out on the walls for the replacement of the radiotherapy equipment showed that it was a nonconventional structure, with only a steel mesh being identified on the inner face.

### 3 | OBJECTIVES

The aim of this study is to study the construction and structural characteristics of the bunker, the characterization

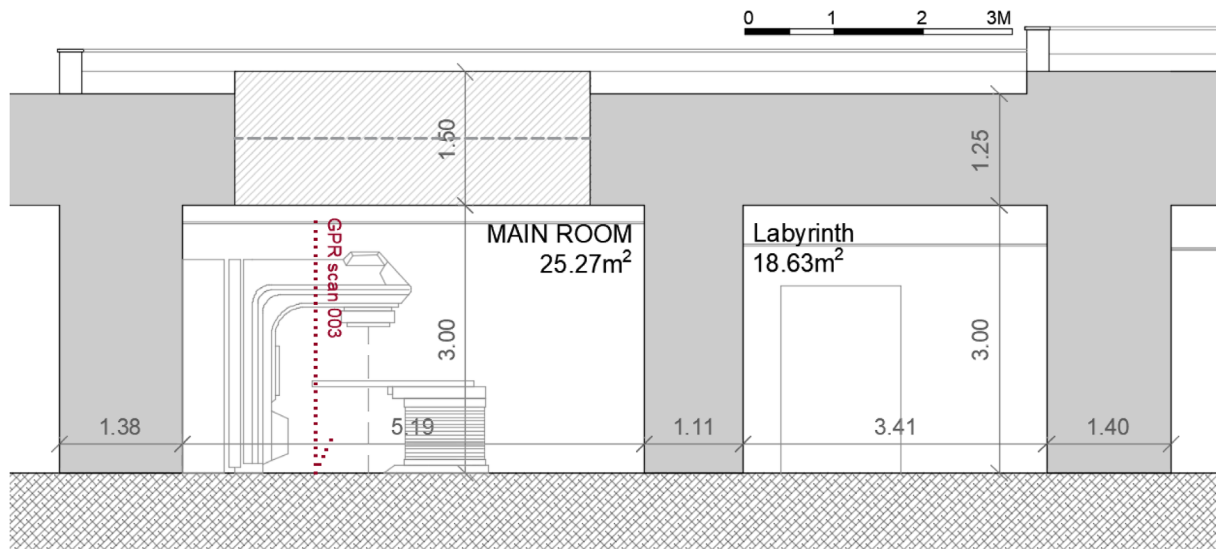


FIGURE 2 Section designed as A-A' in the floor plan



FIGURE 3 (a) Image of the bunker during the execution of the work after the cutting of wall 003. (b) Disassembly of the reinforced concrete wall (wall 003) from the bunker. Steel wire cutting process

of the concrete with which it was built in the 80's and its current state.

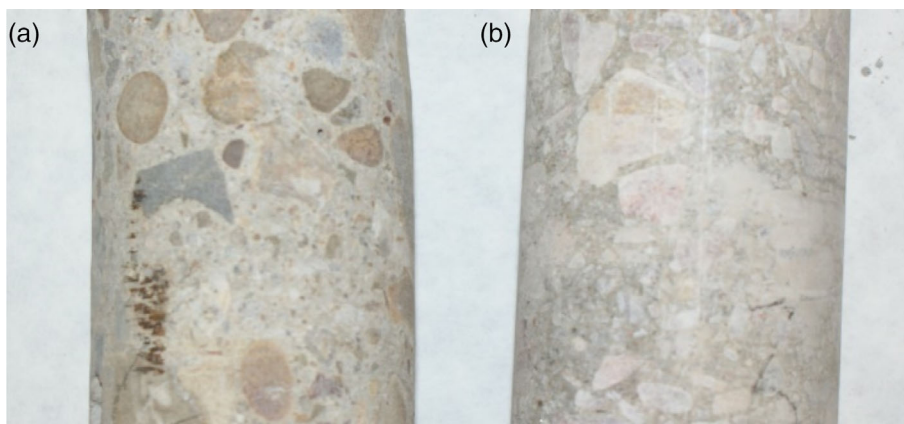
Once the construction element has been evaluated, an evaluation of the impact of the radiation emitted inside the chamber by the linear accelerator on the concrete wall was carried out. For this purpose, a chemical and mineralogical analysis was carried out and the radio-nuclides were quantified. The dismantling of the wall offered the possibility of evaluating the latent radioactive activity in the concrete and the presence of gamma-emitting radioisotopes of activation. The analysis allows to study the state of radioactive activation in which the rest of the concrete elements of the chamber—still in use—are and take a decision about their treatment as waste.

## 4 | MATERIALS AND METHODOLOGY

Once the two concrete sheets of wall 003 were identified, four cylindrical cores of 7 cm in diameter at 1 m from the ground were extracted from the inside to the outside. They were designated as VR1 and VR2 from the first section of the wall; and VR3 and VR4 from the second section (Figures 1 and 4).

The reinforced structure of the bunker walls was evaluated using a PROCEQ GP8800 ground penetrating radar with a defined frequency range between 400 and 6000 MHz and a penetration capacity of up to 65 cm. The data has been processed with the Proceq GPR Live software which allows to read results on-site. Ground

**FIGURE 4** Samples from wall 003.  
(a) Conventional concrete. (b) Barite concrete



penetration radar (GPR) is a nondestructive method that uses extremely high electromagnetic frequency waves (Ultra High Frequency, UHF) aimed at detecting the internal characteristics of a given medium and basically responds to the principle of wave reflection in dielectric discontinuities.<sup>20,21</sup> In this case, it can detect the steel reinforcement of the concrete and evaluate the state of the element, deformations, voids or internal cracks. It also allows the measurement of the dielectric constant of concrete, which is a physical property that indicates, among other things, how fast radar energy travels through the concrete and depends on its water content, age of curing, component, ....<sup>22</sup> Additionally, the equipment has a 3D analysis module that allows to obtain a simulated image of the reinforcement layout and the state of the reinforcement.<sup>23</sup>

Several readings were taken on two of the reinforced concrete walls (wall 001 and 002), in order to determine the reinforcement structure, position of the reinforcement and the dielectric constants (Figure 5). The radar measurements taken from the surface were complemented by measurements with a metal detector model ETI-H0385 to confirm the exact position and depth of the steel bars.

The physical properties related to the porous system of the concrete were determined by measuring the bulk and real density and open porosity of the samples using the vacuum method in accordance with standard UNE 83980, 2014.<sup>24</sup> The compressive strength was carried out on cores by facing both sides, with a loading rate of 50 N/s until failure, in accordance with UNE-EN 12504-1, 2001.<sup>25</sup>

Chemical characterization by X-ray fluorescence was carried out in a Panalytical X-ray fluorescence spectrometer (AXIOS) with Rh tube for elemental analysis of solid samples. Samples were prepared from concrete crushing and splitting as fused beads created by mixing a finely powdered (<63  $\mu\text{m}$ ) sample with a flux mixture of lithium tetraborate (66%)/metaborate (34%) in a flux/sample ratio of 10:1, heated to 900–1000°C in a platinum crucible.

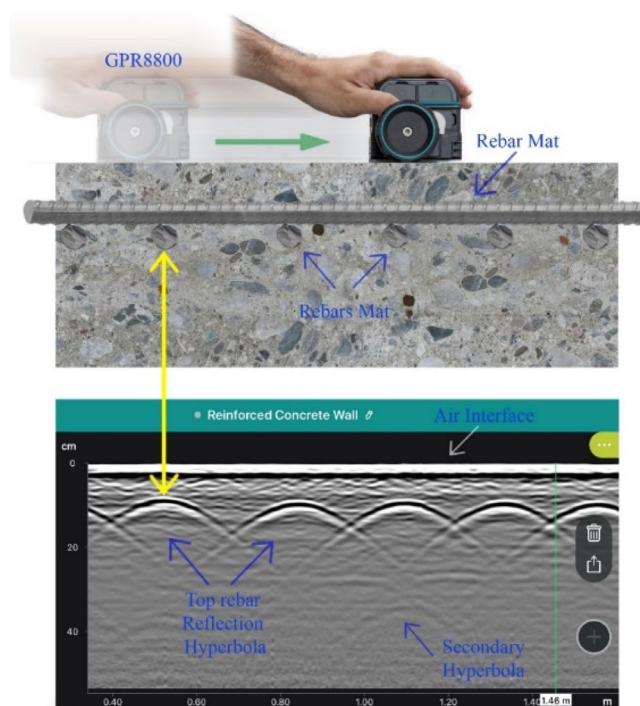


**FIGURE 5** Surface radar detection scheme and reported image

The resultant fused bead is a homogeneous representation of the sample free of mineral structures reducing the mineralogical or matrix effects. The mineralogical characterization was made by X-ray diffraction in a Bruker-AXS diffractometer model D8I-A25, equipped with a Cu  $K\alpha$  copper filament ( $\lambda = 1.5405 \text{ \AA}$ ), with Bragg-Brentano  $\theta$ - $\theta$  configuration, nickel filter and Lynxeye linear detector and the XRD patterns were obtained using the powder technique, at an angle of  $2\theta$ , a range of  $3^\circ$  to  $70^\circ$ , and a  $0.03^\circ$  step scan with a 1 s step. In both cases, samples were previously dried at  $105^\circ\text{C}$  and grounded in a ball mill to a particle size under  $63 \mu\text{m}$ .

To identify the emissions of the possible isotopes present, the concrete samples were analyzed using the gamma spectrometry technique. Gamma activity was

measured with a Canberra Xtra GX4018 detector with a resolution of 1.8 keV for 1.33 MeV, connected to a Canberra DSA-1000 acquisition device, and the spectra obtained were analyzed using Genie2000 software. The counting efficiency was calculated using the EFFTRAN code.<sup>26</sup>

A Berthold LB 124 SCINT contamination monitor was used to measure the surface beta radioactive contamination of cores.<sup>27</sup> It consists of a display unit with micro-processor electronics, signal processing electronics and a

ZnS scintillator with photomultiplier, and with an active measurement area of 345 cm<sup>2</sup>. For the measurement of C-14, it has a counting efficiency of about 30% and a minimum detectable activity (MDA) of 0.23 Bq/cm<sup>2</sup>.

Finally, the samples were analyzed with a Berthold LB 123 dose monitor with a LB 1236-H10 contamination probe attached. This monitor consists of a proportional detector that measures the equivalent dose rate ( $\mu\text{Sv/h}$  H10) at a given distance from the surface of the cores.

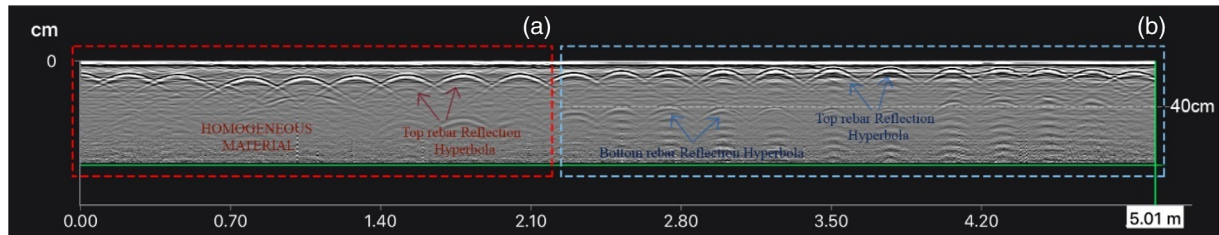


FIGURE 6 Horizontal Radargram, in wall 001

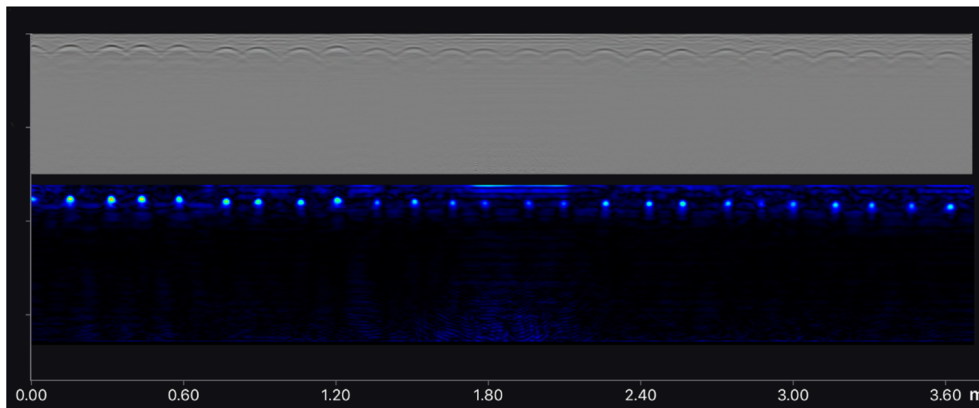


FIGURE 7 Horizontal Radargram from wall 002

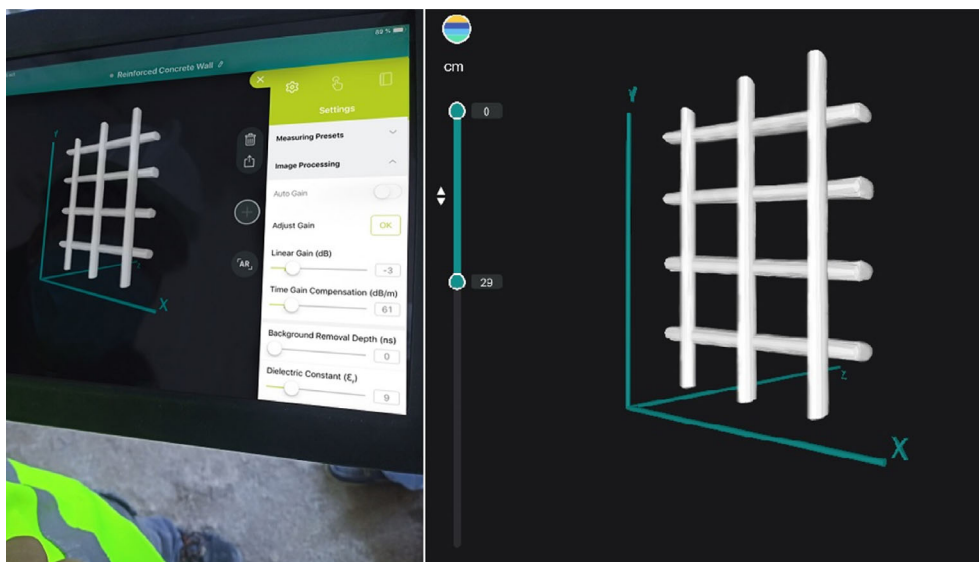


FIGURE 8 Process of obtaining the reinforcement of the concrete wall by means of GPR

TABLE 1 Chemical analysis of majority and minority components

SAMPLE	SiO <sub>2</sub>	Al <sub>2</sub> O <sub>3</sub>	Fe <sub>2</sub> O <sub>3</sub>	MnO	MgO	CaO	Na <sub>2</sub> O	K <sub>2</sub> O	TiO <sub>2</sub>	P <sub>2</sub> O <sub>5</sub>	SO <sub>3</sub>	BaO	CuO	SrO	ZnO	Cl	loi
VR-1	71.96	5.13	2.73	0.12	0.55	11.46	0.96	1.13	0.28	0.07	0.69	-	-	-	-	-	6.23
VR-2	73.60	4.51	1.90	0.05	0.44	10.01	0.66	1.01	0.32	0.11	0.57	-	-	-	-	-	6.29
VR-3	17.30	1.79	1.77	-	0.40	6.88	-	0.40	0.21	0.04	29.13	37.30	0.03	0.76	0.03	-	3.96
VR-4	16.40	1.64	1.93	0.05	0.39	8.06	-	0.35	0.09	-	28.60	37.09	0.04	0.75	0.04	0.08	4.50

Abbreviation: LOI, loss on ignition.

## 5 | ANALYSIS OF RESULTS

### 5.1 | Ground penetrating radar

Figure 6 shows the horizontal linear radargram obtained at 1 m from the ground of wall 001. A deformation in the reinforcement can be identified, longitudinally in the first 2.50 m, reinforcement is detected at an average depth of 8 cm, with an average distance between bars of about 20 cm and a dielectric constant of 10.4. The study allows us to identify a slight deformation in the arrangement of the superficial steel reinforcement, possibly caused by the thrust of the concrete during the concreting phase. Additionally, two different areas are detected and indicated in Figure 8. Area “A” appears to be a unique 1 m thickness wall and area “B” indicates a double wall in which the superficial one has around 0.45 m thickness as indicated in Figure 1. This could indicate that there is a barite concrete wall reinforcement. Currently, this hypothesis cannot be confirmed without carrying out destructive tests on the wall, which is not allowed in this renovation work.

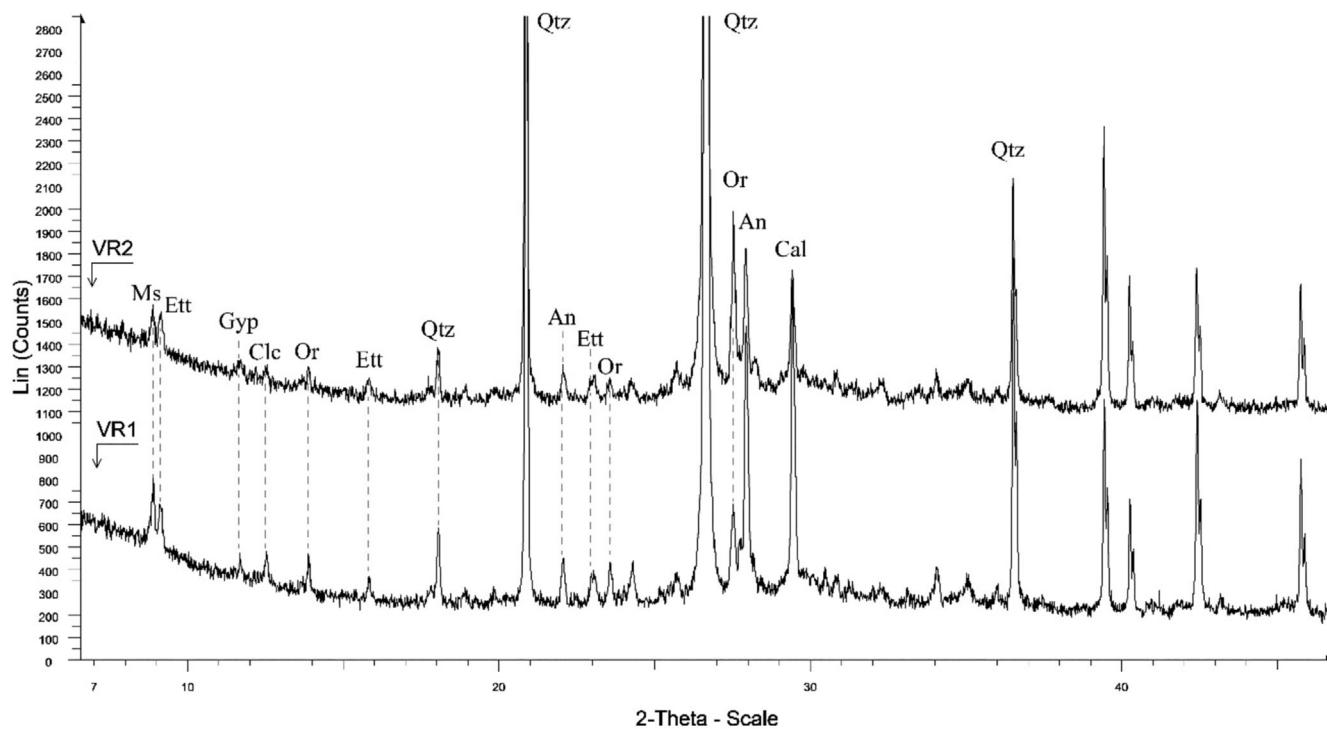
In the case of wall 002, the vertical reinforcement is slightly denser, with bars every 15 cm, maintaining a homogeneous average cover of 4.5 cm and with a dielectric constant of 9. The results obtained for the dielectric constants correspond to values within the range of mature and dry concretes,<sup>28</sup> without allowing any type of anomaly to be established. The position and cover of the horizontal reinforcement of this wall 002 are identical to the vertical reinforcement (Figure 7).

Figure 8 shows the 3D image of the steel structure obtained during the test, showing the homogeneity of the structure, as well as the maintenance of the bar arrangement without detecting any element that could be interpreted as irregular or deterioration.

### 5.2 | Chemical analysis

The chemical analysis (Table 1) shows a clear difference between the samples of both wall layers. The inner one—samples VR1 and VR2—shows the typical composition of a concrete with mostly siliceous aggregate and small differences in all the chemical elements.

On the contrary, samples VR3 and VR4 present a completely different composition with a high barium content, expressed as BaO, higher than 37% and sulfur content of 28% expressed as SO<sub>3</sub>, associated to the incorporation of barite (barium sulphate) as an aggregate to obtain a concrete with a higher specific weight. The SiO<sub>2</sub>, corresponding to another fraction of the aggregate, appears in much smaller quantities.



**FIGURE 9** Samples VR1 and VR2 diffractograms. An, anorthite; Cal, calcite; Clc, clinocllore; Ett, ettringite; Gyp, gypsum; Ms, muscovite; Or, orthoclase; Qtz, quartz

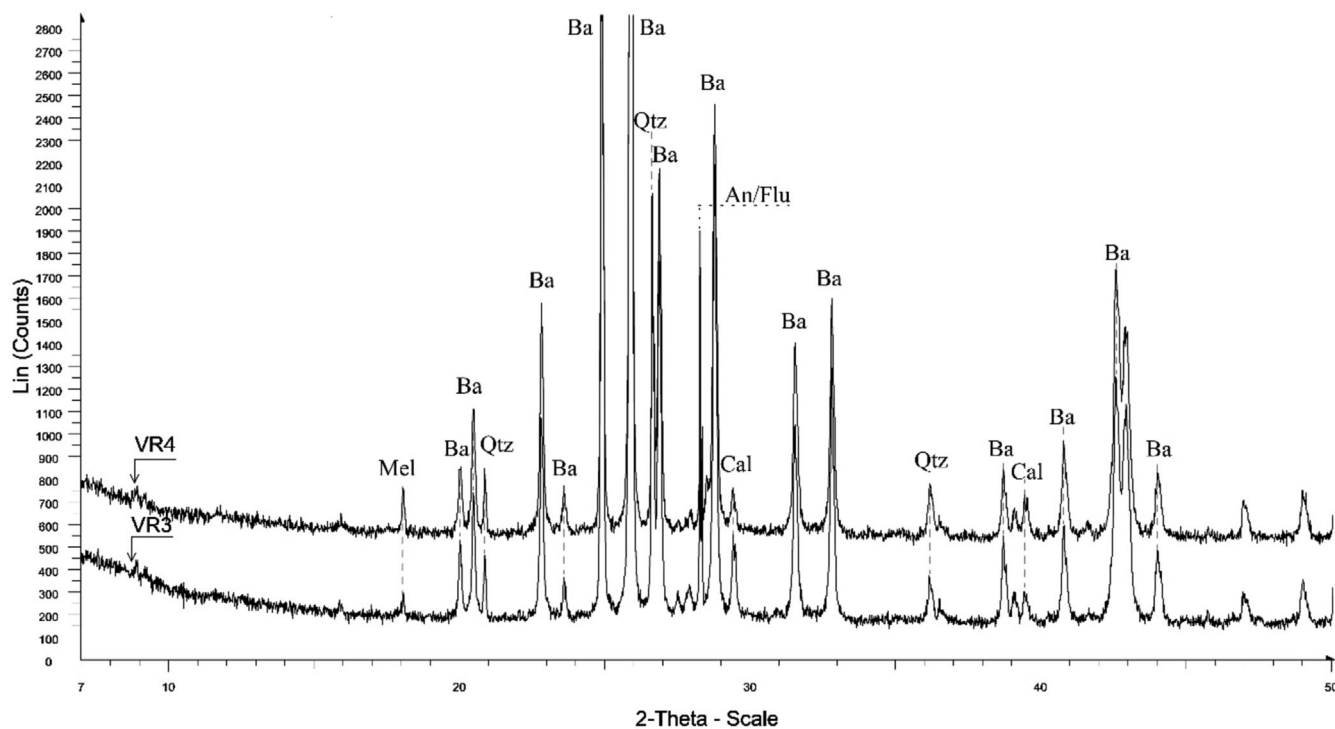


**FIGURE 10** Samples VR3 and VR4 diffractograms. An, anorthite; Ba, barite; Cal, calcite; Flu, fluorite; Mel, melanterite; Qtz, quartz

The trace elements analyzed show logical and very sensitive differences between the samples of the two concretes, with no identifiable anomalies detected.

### 5.3 | Mineralogical analysis

The mineralogical analysis showed a significant difference between the pairs of samples VR1/VR2 and VR3/VR4. Samples VR1 and VR2 show the composition of a conventional siliceous aggregate concrete (Figure 9), with low intensity peaks of phyllosilicates and calcite and an almost negligible intensity peak of portlandite.

XRD of samples VR3 and VR4 show a high intensity peak corresponding to barite, which is associated with the low intensity of the quartz peak. The presence of calcite is not very significant. It is worth noting the identification in both samples of the peak corresponding to fluorite, a mineral phase that usually appears associated with barite (Figure 10).

### 5.4 | Physical and mechanical properties

The physical properties obtained fully confirm the theoretical definition of the concretes used to build the walls (Table 2). The porosity of both concretes is similar, which

gives an idea that the w/c ratio and the degree of compaction have been similar in both cases. This factor is very relevant in the effectiveness of the chamber, since abnormal heterogeneity of the concrete can cause local radiation peaks and these cases must be effectively avoided.<sup>4</sup> It has been confirmed that the bulk density of the outer sheet is significantly higher ( $\approx 50\%$ ), which confirms the influence of the aggregate density on the concrete density. With regard to the real density values, it should be noted that the value obtained for the conventional concrete samples is fully consistent with the density of quartz ( $2.65 \text{ g/cm}^3$ ) and calcite ( $2.7 \text{ g/cm}^3$ ), minerals present in the aggregate; while, for the concrete with barite, the real density is close to that of the majority mineral ( $4.48 \text{ g/cm}^3$ ).

The compressive strength test revealed that barite concrete develops lower strength than conventional one. Compressive strength and tensile strength values decrease proportionally to the barite content.<sup>6</sup> This difference is particularly due to the crystalline structure of barite,<sup>29</sup> which microstructure is composed of adjacent layers with interfaces. The performance of concrete is conditioned by the friability and the cracking pattern experienced by the barite under compression due to delamination at reduced compressive strengths.<sup>30</sup>

It is important to note that, for this type of element, compressive strength is not a particularly relevant factor, as they are not load-bearing structures.

**TABLE 2** Average values of physical and mechanical properties

	Pa (%)	Da ( $\text{gr/cm}^3$ )	Dr ( $\text{gr/cm}^3$ )	Compressive strength (MPa)
VR1/VR2	17.20	2.20	2.65	42.35
VR3/VR4	17.47	3.16	3.83	18.80

**TABLE 3** Activity concentrations (Bq/kg) and their uncertainties obtained by gamma spectrometry for the VR1 and VR2 samples

Radioisotope	E (KeV)	VR1			VR2		
		A (Bq/kg)	err	AMD (Bq/kg)	A (Bq/kg)	err	AMD (Bq/kg)
Th-234	63.3	20.3	4.9	15.4	14.5	4.6	14.4
Pb-214	351.9	16.3	0.1	1.9	9.2	0.8	1.9
Pb-210	46.5	16.4	2.9	19.1	16.5	2.7	16.9
Ra-224	241	24.5	2.7	9.1	22.5	2.5	8.3
Pb-212	238.6	20.9	1.3	1.4	16.5	1.1	1.5
Bi-212	727.3	17.7	1.7	9.1	16.8	1.6	8.8
Ac-228	338.3	19.8	0.7	2.7	16.9	0.2	2.6
Tl-208	583.2	17.4	0.4	2.2	14.8	0.2	2.5
K-40	1460.8	321	18	11	223	13	10
Cs-137	661.6	<MDA		0.75	<MDA		0.60
Co-60	1332.5	<MDA		0.44	<MDA		0.41
Eu-152	964.0	<MDA		0.56	<MDA		0.53

Abbreviation: MDA, minimum detectable activity for the technique.

Radioisotope	E (KeV)	VR3			VR4		
		A (Bq/kg)	err	A (Bq/kg)	err	A (Bq/kg)	err
Th-234	63.3	30.6	25.7	30.6	25.7	30.6	25.7
Pb-214	351.9	6.6	0.1	6.6	0.1	6.6	0.1
Pb-210	46.5	32.7	22.8	32.7	22.8	32.7	22.8
Ra-224	241	4.2	1.5	4.2	1.5	4.2	1.5
Pb-212	238.6	5.9	0.6	5.9	0.6	5.9	0.6
Bi-212	727.3	5.9	1.0	5.9	1.0	5.9	1.0
Ac-228	338.3	6.5	0.7	6.5	0.7	6.5	0.7
Tl-208	583.2	5.6	0.3	5.6	0.3	5.6	0.3
K-40	1460.8	84	6	84	6	84	6
Cs-137	661.6	<MDA		<MDA		<MDA	
Co-60	1332.5	<MDA		<MDA		<MDA	
Eu-152	964.0	<MDA		<MDA		<MDA	

Abbreviation: MDA, minimum detectable activity for the technique.

TABLE 5 Obtained dose for analyzed samples ( $\mu\text{Sv/h H10}$ )

Sample	Dose ( $\mu\text{Sv/h H10}$ )
VR1	0.115
VR2	0.118
VR3	0.124
VR4	0.122

## 5.5 | Gamma spectrometry

The results obtained from gamma spectrometry are shown in Tables 3 and 4. It can be seen that no activating gamma-emitting radioisotope has been detected for any of the cores analyzed. On the other hand, it is observed that the activity concentrations (Bq/kg) for the natural radioisotopes intrinsically contained in the concrete material itself (and not activated) are different for the cores VR1 and VR2, and VR3 and VR4. This allows us to differentiate between the concrete with and without barite. In any case, the levels obtained are within the expected range for concrete.<sup>31</sup>

For the C-14 isotope, measurements on the four samples showed activity values lower than MDA, so it can be assumed that they are free of this radioisotope. This surface concentration is below the established level of  $0.4 \text{ Bq/cm}^2$ , so the residual material is not impacted.<sup>32</sup>

In the measurements of equivalent dose rates ( $\mu\text{Sv/h H10}$ ; Table 5), at a given distance from the surface, all values did not exceed the legal limit of  $2 \mu\text{Sv/h}$ .<sup>33</sup>

The obtained results can be explained by taking into account that the threshold energy of the reactions ( $\gamma, n$ ) is 8.5 MeV for heavy cores (i.e., for Pb, W, etc.) and about 10 MeV for most of the isotopes of lower atomic number present in the materials.<sup>33</sup> In this case, the energy of the dismantled LINAC was 6 MeV, so, despite the time

TABLE 4 Activity concentrations (Bq/kg) and their uncertainties obtained by gamma spectrometry for the VR3 and VR4 samples

elapsed, no activation has occurred in the concrete materials in the bunker. This material can be declassified as it is below the levels established in the current legislation.

## 6 | CONCLUSIONS

The analysis of the bunker structure has revealed a unique structure, made with two types of concrete, in order to guarantee the capacity for radioactive insulation without generating a general overload of the walls. This has been done with a double sheet structure of conventional concrete and barite concrete. The GPR analysis ensures that no alterations have occurred in the steel reinforcement bars, and also rules out the development of alterations within the concrete. Thanks to the presence of the top & bottom rebars visualized in radargrams it was confirmed the existence of a two-leaf concrete wall. The position of the rebars and the logical idea of repeat the same execution as the analyzed wall could implies that a second barite concrete wall is located in the opposite side of the room. Thus, GPR could confirm the reinforcement of radiation protection without carrying out destructive tests on the wall.

The analysis and testing methodology developed makes it possible to assess the potential risk of this type of material at the end of its service life, as well as the radiation attenuation capacity of the concrete walls. The values obtained for the porosity, densities and mechanical strength are within the usual range for this type of material. Likewise, the chemical and mineralogical analyses, beyond the differences between the two concretes, have shown that no alteration of any kind has occurred in the materials.

The levels of radioactive activity in the concrete are in all cases within the legal limits for concrete residues, with

no gamma-emitting radioisotopes of activation having been detected. Likewise, the C-14 values and equivalent dose rates in all the cases were below the legal limits, allowing to affirm that the dismantled concretes do not pose any environmental risk.

The treatment of the dismantled concrete as waste does not pose any problem from the radiological and environmental point of view. Therefore, it could be assumed that the state of the preserved parts of the structure does not present any type of radioactive activity that could be dangerous.


## ACKNOWLEDGMENTS

This research has been carried out thanks to the financing of the project PGC2018-093470-B-I00 of the Ministry of Science, Innovation and Universities of the Government of Spain. The authors also wish to express their gratitude to the CITIUS at the University of Seville.

## DATA AVAILABILITY STATEMENT

Data sharing is not applicable to this article as no new data were created or analyzed in this study.

## ORCID

Vicente Flores-Alés  <https://orcid.org/0000-0003-4329-0020>

## REFERENCES

- Ongaro C, Zanini A, Nastasi U, Rodenas J, Ottaviano G, Mafredotti C. Analysis of photoneutron spectra produced in medical accelerators. *Phys Med Biol*. 2000;45(12):L55–61. <https://doi.org/10.1088/0031-9155/45/12/101>
- Price KW, Nath R. Fast and thermal neutron profiles for a 25-MV x-ray beam. *Med Phys*. 1978;5(4):285–9. <https://doi.org/10.1118/1.594479>
- Vega-Carrillo HR, Barquero R, Méndez R, Iñiguez MP, Manzanares-Acuña E. Campos neutrónicos producidos por un acelerador lineal para radioterapia. *Rev Med Nucl Alasbimn J*. 2007;9(36).
- Kubissa W, Glinicki MA, Dąbrowski M. Permeability testing of radiation shielding concrete manufactured at industrial scale. *Mater Struct Constr*. 2018;51(4):1–15. <https://doi.org/10.1617/s11527-018-1213-0>
- Ling TC, Poon CS, Lam WS, Chan TP, Fung KKL. X-ray radiation shielding properties of cement mortars prepared with different types of aggregates. *Mater Struct Constr*. 2013;46(7):1133–41. <https://doi.org/10.1617/s11527-012-9959-2>
- Esen Y, Yilmazer B. Investigation of some physical and mechanical properties of concrete produced with barite aggregate. *Sci Res Essays*. 2010;5(24):3826–33.
- Kilincarslan S, Akkurt I, Basyigit C. The effect of barite rate on some physical and mechanical properties of concrete. *Mater Sci Eng A*. 2006;424:83–6. <https://doi.org/10.1016/j.msea.2006.02.033>
- Topçu IB. Properties of heavyweight concrete produced with barite. *Cem Concr Res*. 2003;33(6):815–22. [https://doi.org/10.1016/S0008-8846\(02\)01063-3](https://doi.org/10.1016/S0008-8846(02)01063-3)
- Glasstone S, Sesonske A. Nuclear reactor engineering. 4th ed. US: Springer; 1994.
- Akkurt I, Akyıldırım H, Mavi B, Kilincarslan S, Basyigit C. Photon attenuation coefficients of concrete includes barite in different rate. *Ann Nucl Energy*. 2010;37(7):910–4. <https://doi.org/10.1016/j.anucene.2010.04.001>
- Bouzarjomehri F, Bayat T, Dashti R, Gheysari J, Abdoli N.  $^{60}\text{Co}$   $\gamma$ -ray attenuation coefficient of barite concrete. *Int J Radiat Res*. 2006;4(2):71–5.
- Israngkul-Na-Ayuthaya I, Suriyapee S, Pengvanich P. Evaluation of equivalent dose from neutrons and activation products from a 15-MV X-ray LINAC. *J Radiat Res*. 2015;56(6):919–26. <https://doi.org/10.1093/jrr/rrv045>
- Vega-Carrillo HR, de Leon-Martinez HA, Rivera-Perez E, Benites-Rengifo JL, Gallego E, Lorente A. Induced radioisotopes in a linac treatment hall. *Appl Radiat Isot*. 2015;102:103–8. <https://doi.org/10.1016/j.apradiso.2015.05.004>
- Martínez-Serrano JJ, de Los D, Ríos A. Prediction of neutron induced radioactivity in the concrete walls of a PET cyclotron vault room with MCNPX. *Med Phys*. 2010;37(11):6015–21. <https://doi.org/10.1118/1.3505919>
- Fujibuchi T, Nohtomi A, Baba S, Sasaki M, Komiya I, Umedzu Y, et al. Distribution of residual long-lived radioactivity in the inner concrete walls of a compact medical cyclotron vault room. *Ann Nucl Med*. 2015;29(1):84–90. <https://doi.org/10.1007/s12149-014-0918-6>
- Endo A, Harada Y, Kawasaki K, Kikuchi M. Measurement of depth distributions of  $^3\text{H}$  and  $^{14}\text{C}$  induced in concrete shielding of an electron accelerator facility. *Appl Radiat Isot*. 2004;60(6):955–8. <https://doi.org/10.1016/j.apradiso.2004.01.010>
- Žagar T, Ravnik M. Determination of long-lived neutron activation products in reactor shielding concrete samples. *Nucl Technol*. 2002;140(1):113–26. <https://doi.org/10.13182/NT02-A3327>
- Perez-Calatayud J, Corredoira S, Crispin C, Eudaldo P, Frutos B, Pino S, et al. Radiation protection in brachytherapy. Report of the SEFM task group on brachytherapy. *Rev Fis Med*. 2015;16(2):11–47.
- OIEA. Seguridad Radiológica De Las Instalaciones De Irradiación De Rayos Gamma, Electrones Y Rayos X. n° SSG-8 (2015).
- Barrile V, Pucinotti R. Application of radar technology to reinforced concrete structures: a case study. *NDT & E Int*. 2005;38(7):596–604. <https://doi.org/10.1016/j.ndteint.2005.02.003>
- Laurens S, Balayssac JP, Rhazi J, Klysz G, Arliguie G. Non-destructive evaluation of concrete moisture by GPR: experimental study and direct modeling. *Mater Struct*. 2005;38(9):827–32. <https://doi.org/10.1007/bf02481655>
- Hasan MI, Yazdani N. Ground penetrating radar utilization in exploring inadequate concrete covers in a new bridge deck. *Case Stud Constr Mater*. 2014;1:104–14. <https://doi.org/10.1016/j.cscm.2014.04.003>
- Lovera, G. Estudio en Estructuras de Hormigón Armado Mediante el Uso de un Radar de Penetración Terrestre. Doctoral Thesis. Univ. Austral de Chile (2006).
- UNE-EN 83980. Concrete durability. Test methods. Determination of the water absorption, density and accessible porosity for water in concrete (2014)
- UNE-EN 12504-1. Testing concrete in structures. Part 1: Cored specimens. Taking, examining and testing in compression (2019)
- Vidmar T. EFFTRAN: a Monte Carlo efficiency transfer code for gamma-ray spectrometry. *Nucl Inst Meth Phys Res Sect A Accel Spectrometers, Detect Assoc Equip*. 2005;550(3):603–8. <https://doi.org/10.1016/j.nima.2005.05.055>

27. Klett, A.; Haefner, P. & Reuter, W. (2005) A new contamination monitor with scintillation detection. In: IEEE Nuclear Science Symposium conference record. Nuclear Science Symposium 2, 1213–1214. <https://doi.org/10.1109/NSSMIC.2005.1596468>.
28. Cao Y, Dai S, Labuz JF, Pantelis J. Implementation of ground penetrating radar. Manhattan/NY: Local Road Research Board, Minnesota; 2007.
29. Widanagamage I, Waldron A, Glamoclija M. Controls on barite crystal morphology during abiotic precipitation. *Minerals*. 2018;8(11):480. <https://doi.org/10.3390/min8110480>
30. González-Ortega MA, Cavalaro SHP, Aguado A. Influence of barite aggregate friability on mixing process and mechanical properties of concrete. *Construct Build Mater*. 2015;74:169–75. <https://doi.org/10.1016/j.conbuildmat.2014.10.040>
31. Chinchón-Payá S, Piedecausa B, Hurtado S, Sanjuán MA, Chinchón S. Radiological impact of cement, concrete and admixtures in Spain. *Radiat Meas*. 2011;46(8):734–5. <https://doi.org/10.1016/j.radmeas.2011.06.020>
32. I. IS-31. Instrucción IS-31. Consejo de Seguridad Nuclear, sobre los criterios para el control radiológico de los materiales residuales generados en las instalaciones nucleares (2011).
33. Maringer FJ, Šurán J, Kovář P, Chauvenet B, Peyres V, García-Toraño E, et al. Radioactive waste management: review on clearance levels and acceptance criteria legislation, requirements and standards. *Appl Radiat Isot*. 2013;81:255–60. <https://doi.org/10.1016/j.apradiso.2013.03.046>

## AUTHOR BIOGRAPHIES



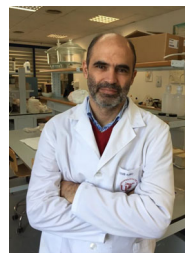
Marta Torres-González, Department of Civil Engineering, Architecture, and Georesources, IST, University of Lisbon, Lisboa, Portugal.



Juan Mantero, Applied Physic II Department, Universidad de Sevilla, Seville, Spain.



Santiago Hurtado, Applied Physic II Department, Universidad de Sevilla, Seville, Spain.



Vicente Flores-Alés, Department of Architectural Constructions II, Universidad de Sevilla, Seville, Spain.



Francisco J. Alejandro, Department of Architectural Constructions II, Universidad de Sevilla, Seville, Spain.



Juan M. Alducín-Ochoa; Department of Architectural Constructions II, Universidad de Sevilla, Seville, Spain.

**How to cite this article:** Torres-González M, Mantero J, Hurtado S, Flores-Alés V, Alejandro FJ, Alducín-Ochoa JM. Characterization and radioactive evaluation of the concrete from a radiotherapy bunker. *Structural Concrete*. 2022; 1–12. <https://doi.org/10.1002/suco.202100379>